Applied Catalysis B: Environmental 166–167 (2015) 91–103

Contents lists available at ScienceDirect

Applied Catalysis B: Environmental

journal homepage: www.elsevier.com/locate/apcatb

Low-temperature CO oxidation by Pd/CeO_2 catalysts synthesized using the coprecipitation method

E.M. Slavinskaya[a,c], R.V. Gulyaev[a,c], A.V. Zadesenets[b,c], O.A. Stonkus[a,c], V.I. Zaikovskii[a,c], Yu. V. Shubin[b,c], S.V. Korenev[b,c], A.I. Boronin[a,c,*]

[a] Boreskov Institute of Catalysis SB RAS, Prosp. Akad. Lavrentieva 5, Novosibirsk 630090, Russia
[b] Nikolaev Institute of Inorganic Chemistry SB RAS, Prosp. Akad. Lavrentieva 3, Novosibirsk 630090, Russia
[c] Novosibirsk State University, Pirogova 2, Novosibirsk 630090, Russia

ARTICLE INFO

Article history:
Received 29 August 2014
Received in revised form 30 October 2014
Accepted 8 November 2014
Available online 15 November 2014

Keywords:
Low-temperature CO oxidation
Pd/CeO_2
Coprecipitation
XPS
TEM

ABSTRACT

Pd/CeO_2 catalysts synthesized using the coprecipitation method under a wide range of palladium loading and calcination temperatures were investigated in this study. Structural (XRD, TEM), spectroscopic (XPS) and kinetic (TPR-CO) methods were used to investigate the morphological and structural forms of the catalysts and identify the states of palladium as the active component on the CeO_2 surface and in its bulk. It was found that the synthesis and subsequent calcination at 450 °C resulted in the formation of two main types of the catalyst components: PdO nanoparticles and $Pd_xCe_{1-x}O_{2-\delta}$ solid solution. Application of HRTEM allowed to establish the formation of aggregates where ceria or $Pd_xCe_{1-x}O_{2-\delta}$ nanoparticles were located around PdO nanoparticles. A subsequent calcination process resulted in partial dissolution of PdO nanoparticles in ceria lattice and formation of the surface compounds of palladium and ceria, PdO_x(s)/Pd–O–Ce(s), which contain high reactive oxygen according to the TPR-CO data. Based on the XPS and TPR-CO data the catalytic activity at low temperatures (<100 °C) was determined by a combination of both palladium surface structures PdO_x(s)/Pd–O–Ce(s) and palladium ions Pd^{2+} in the $Pd_xCe_{1-x}O_{2-\delta}$ bulk phase.

1. Introduction

There is great interest in supported Pd/CeO_2 catalysts due to their wide range of applications, such as the neutralization of automotive exhausts, room air purification by the low-temperature oxidation of CO (LTO CO), and development of catalytic gas sensors [1–11].

The effect of the palladium content on its state on the surface of the CeO_2 support and the catalytic characteristics of Pd-supported catalysts in CO oxidation has been considered in a series of studies. As reported in [12], an increase in the Pd content improves the performance of Pd/CeO_2 catalysts. However, there is no agreement on the state of the Pd present on the CeO_2 support. Opinions on the Pd state at low concentrations also vary. According to [12], the palladium on the surface of CeO_2 calcined at 650 °C is present as palladium hydroxide, and its content in the catalyst ranges from 0.25% and 0.75%. Increasing the Pd content to 2% leads to appearance of a finely dispersed PdO phase, while increasing it to 5% produces a coarse PdO phase. Using the obtained data, the authors concluded that the active phase of Pd/CeO_2 catalysts is represented by palladium hydroxide. An investigation of Pd/CeO_2 with a high Pd content (10 wt.%) showed that PdO is the catalytically active species and that the oxidation of CO is accompanied by the formation of small amounts of metallic palladium and palladium oxide [13].

The formation of cationic Pd species due to the strong interaction of Pd with CeO_2 in Pd/CeO_2 catalysts was observed in most previous studies [8–10,14–21]. It was shown that the strong interaction of Pd with CeO_2 results in the formation of $Ce_{1-x}Pd_xO_{2-(4-n)x/2}$ solid solution with $-O^{2-}-Ce^{4+}-O^{2-}-M^{n+}-O^{2-}$ ($n = 2, 4$) type bonds on the surface of CeO_2 [3]. The authors suggested that the Pd^{2+} ions in the CeO_2 matrix are the active sites of the low-temperature oxidation of CO [3,9]. Additionally, the formation of cationic Pd species takes place even at a very high Pd content (17 wt.%) [22]. PdO_x ($x = 1–2$) and $Ce_{1-x}Pd_xO_{2-\delta}$ solid solution were also formed in the catalyst synthesized by a solution combustion method [20]. It was found that the surface PdO_x species could be removed by nitric acid treatment. Also, a part of Pd^{4+} cations in the CeO_2 lattice migrated to the surface to form surface PdO_x species after high

* Corresponding author at: Boreskov Institute of Catalysis SB RAS, Prosp. Akad. Lavrentieva 5, Novosibirsk, 630090, Russia. Tel.: +7 3833269631; fax: +7 3833308056.
E-mail address: boronin@catalysis.ru (A.I. Boronin).

http://dx.doi.org/10.1016/j.apcatb.2014.11.015
0926-3373/

temperature calcination (500 °C). For CO oxidation, the specific reaction rate of the surface PdO_x species was 249 times higher than of the $Ce_{1-x}Pd_xO_{2-\delta}$ solid solution, due to the fact that the surface PdO_x species provided CO chemisorption sites.

A wide spectrum of opinions regarding Pd species on the surface of CeO_2 can be attributed to various factors, particularly the conditions of the support synthesis and treatment, the method of palladium deposition and subsequent treatment of the catalysts, the nature of the precursor of supported palladium, the palladium content in the catalysts, faceting of the nanoparticles, the local structure of the support surface, and the action of the reaction medium. It should be noted that the catalysts synthesized using the solution-combustion method comprise mainly cationic palladium species [3,10,23]. When other methods are used for the synthesis, such as deposition–precipitation or incipient wetness impregnation [12,13,18], small particles of PdO and metallic Pd are present in addition to the cationic palladium species. It is also important to note that different crystallinites of the CeO_2 supports affects the formation of ionic palladium species, which was reported in [24]. In that study, CeO_2 samples synthesized by precipitation and calcined at 450–600 °C had a high concentration of point defects, and catalysts based on this ceria showed a high catalytic activity.

In our previous studies [25,26], the CeO_2 supports were synthesized using three methods: (1) the thermal decomposition of the nitrate in air under conditions of temperature-programmed heating to 450 °C, (2) the precipitation of CeO_2 with ammonium hydrogen carbonate, and (3) the precipitation of CeO_2 with an aqueous ammonia solution. Palladium was deposited by the standard impregnation method from a palladium nitrate solution. It was shown that the Pd/CeO_2 catalyst with a high low-temperature activity (T_{10} = 17 °C) comprises two palladium species: the surface interaction phase ($Pd_xCe_{1-x}O_{2-\delta}$) and small oxidized PdO_x clusters (<1 nm), which have a flattened shape due to epitaxial binding to CeO_2. A decrease in the low-temperature activity for the oxidation of CO (T_{10} = 100 °C) is caused by a loss of the chemical interaction of palladium with the support surface and by an abrupt coarsening of the palladium particles with the formation of PdO nanoparticles [25]. This finding suggests that a high concentration of defects and a certain structure of the support surface allow the cationic palladium species to form even with the standard impregnation from a palladium nitrate solution. In addition to the cationic palladium species, extremely small and partially oxidized palladium clusters are formed on the support surface.

It follows from the results considered above that when palladium is deposited on the ceria surface, for example, by impregnation, it is stabilized as a cationic species due to dissolution in the subsurface layers of the support. Thus, the synthesized catalysts are expected to be metastable because the process of palladium dissolution can extend over the entire bulk, which decreases the surface concentration of the active component and, accordingly, the activity. Due to this connection, it seems quite natural to establish a relationship between the palladium concentration (loading) and its location on the surface/in the bulk. Unfortunately, our analysis of the literature and our own results did not allow us to make an unambiguous conclusion about the effect of the palladium concentration on its state at the surface of the CeO_2 support and its catalytic properties. Thus, the aim of this work was to investigate Pd/CeO_2 catalysts synthesized using the coprecipitation method with varying palladium content. Essentially, the coprecipitation method is able to initially produce the required condition for the stabilization of palladium in its ionic form directly in the CeO_2 lattice. A set of physicochemical methods for analyzing both the bulk and surface of the samples can be used to reveal more accurately the location of palladium in Pd/CeO_2 catalysts. This will allow us to relate the observed states with the catalytic activity and, ultimately, to determine both the amount of palladium located in the bulk for stabilization of the mixed structures and the amount residing on the surface for the formation of active sites efficient in the low-temperature oxidation of CO.

2. Experimental

2.1. Catalysts

The calculated amount of metallic palladium was dissolved in a minimum necessary amount of nitric acid; the resulting solution was cooled and supplemented with the calculated amount of cerium (III) nitrate. The reactant ratios were calculated so as to obtain the target Pd content in the catalyst in terms of non-aqueous supported Pd/CeO_2 sample. The Pd:Ce molar ratios of 1:99, 5:95 and 10:90 were prescribed in advance. The exact Pd concentration in the samples determined by atomic absorption spectrometry (AAS) was equal to 0.74, 3.8 and 7.7 wt.%.

A mixed solution of cerium and palladium nitrates was added dropwise to a 1 M solution of alkali (NaOH) under stirring. This resulted in the formation of a hydroxide precipitate $PdO{\cdot}nCe_2O_3{\cdot}mH_2O$. The introduction of the last portions of the mixed solution, when the alkali has been consumed and pH decreased, was accompanied by the reduction of palladium presumably by the reaction

$$Pd^{2+} + 2Ce^{3+} + 4H_2O \rightarrow Pd + 2CeO_2 + 8H^+$$

The obtained precipitates (3.8 and 7.7 wt.% Pd) were separated on a filter and washed with water. A precipitate with the lowest palladium content (0.74 wt.% Pd) was separated by a five-fold centrifuging due to high dispersion. The samples were dried at 120 °C and calcined at 450, 600 and 800 °C in flowing oxygen. The samples were designated as n%Pd/CeO_2-T, where n% is the weight percent of palladium in the sample, and T is the calcination temperature, °C.

Specific surface areas of the samples are listed in Table 1.

2.2. Methods of investigation

Atomic absorption spectrometry (AAS) was used for the determination of the concentrations of the main components of the catalysts [27].

The specific surface of samples S_{BET} was determined by argon thermal desorption using a Sorbtometr-M adsorption analyzer. The measurement error of the method was 10% [28].

X-ray photoelectron spectroscopy (*XPS*) was performed using an ES-300 (KRATOS Analytical) photoelectron spectrometer equipped with MgK_α ($h\nu$ = 1253.6 eV) radiation sources. The spectrometer was calibrated using the $Au4f_{7/2}$ (84.0 eV) and $Cu2p_{3/2}$ (932.7 eV) lines of pure metallic surfaces of gold and copper. The U''' component of the Ce3d spectral line (E_b = 916.7 eV) served as a standard for the calibration of XPS spectra. A homemade software package, XPS-Calc, was used for the mathematical treatment of the XPS spectra. This software has been previously applied for different samples [29–31], including Pd/CeO_2 and Pd/Al_2O_3 catalysts [25,26]. The Shirley model and Gauss–Lorentz functions were used for background subtraction and curve fitting, respectively.

X-ray diffraction (*XRD*) was carried out using CuK_α radiation on a DRON-SEIFERT-RM4 diffractometer that was equipped with a graphite monochromator on the reflected beam and a scintillation detector with amplitude discrimination. A polycrystalline silicon sample (a = 5.4309 Å) prepared in a similar way was used as the external reference. The diffraction patterns were recorded in a stepwise manner, with accumulations required to record the reflections of small phases. The size of the crystallites was determined from the

Table 1
XRD data and S_{BET}.

Catalysts	$T_{calcination}$, °C	S_{sp}, m^2/g	Phase	Crystallite size, nm	Crystal lattice parameters of CeO_2 ±0.002, Å
PDF – 34-394			CeO_2		5.411
0.74%Pd/CeO_2	450	71	CeO_2	7.6	5.414
	600	70	CeO_2	7.7	5.412
	800	18.5	CeO_2	22	5.414
3.8%Pd/CeO_2	450	118	CeO_2	6.7	5.414
	600	75	CeO_2	7.7	5.412
	800	25	CeO_2	16.9	5.412
7.7%Pd/CeO_2	450	127	CeO_2	5.8	5.411
			PdO	~8	
	600	107	CeO_2	6.8	5.411
			PdO	~9	
	800	25	CeO_2	17	5.417
			PdO	~25	

integral broadening of isolated diffraction profiles by the Scherrer formula using the WINFIT 1.2.1 software [32].

Investigation of catalytic properties of the synthesized samples was performed in an automated setup with a flow reactor and mass-spectrometric analysis of the gas mixture using the temperature-programmed reaction (light-off). A sample with the particle size of 0.25–0.5 mm was mounted in a stainless steel reactor. The reaction mixture containing 0.2 vol.% CO, 1.0 vol.% O_2, 0.5 vol.% Ne, and helium the balance was fed at a rate of 1000 cm^3/min to the initial catalyst cooled to −10 °C. The catalyst was heated in the reaction mixture from −10 °C to 450 °C at a rate of 10 °C/min with subsequent cooling and repeated heating in the reaction mixture. The concentrations of CO, O_2 and CO_2 were monitored in the course of reaction at a frequency of 0.34 Hz. The reaction rate and activation energy were estimated for CO conversions up to 20% using the formula W (molecules/cm^2 × s) = $(C^0_{CO} \times X \times V_{RM})/(m \times S_{sp})$, where C^0_{CO} is the initial concentration of CO (molecules/cm^3), X is the CO conversion, V_{RM} is the reaction mixture rate (cm^3/s), m is the weight of a sample (g), and S_{sp} is the specific surface area (cm^2/g).

TPR-CO method. The reaction mixture containing 1.0 vol.% CO, 0.5 vol.% Ne and helium the balance was introduced at a flow rate of 100 cm^3/min to the catalyst sample (0.2 g) preliminary cooled in the reactor to −10 °C. As the steady-state concentrations of CO and CO_2 were established, the sample was heated from −10 to 450 °C at 10 °C/min heating rate. The concentrations of CO, CO_2, O_2, H_2 and H_2O were measured during the reaction. Before each TPR-CO experiment the catalysts were pretreated by 20%O_2/He gas mixture at 450 °C during 2 h with subsequent cooling in this mixture.

Electron microscopy investigation was performed using JEM-2010 (JEOL Co., Japan) and JEM-2200FS (JEOL Co., Japan) electron microscopes operated at 200 kV for obtaining HRTEM images. STEM HAADF mode was employed together with EDX spectroscopy. The samples for the TEM study were prepared on the perforated carbon film mounted on a copper grid.

3. Results

3.1. Catalytic properties

Fig. 1 displays the temperature dependencies of CO conversion (Fig. 1a, c, and e) and the CO oxidation rate in Arrhenius coordinates (Fig. 1b, d, and f) for Pd/CeO_2 catalysts containing 0.74, 3.8, and 7.7%Pd and calcined at 450, 600, and 800 °C. For the 0.74%Pd/CeO_2 catalysts calcined at 450 and 600 °C, deceleration of the conversion growth in the temperature region of 90–130 °C is observed on the CO conversion curve. The values of T_{10} are equal to 52, 42, and 33 °C, and those of T_{50} are 129, 124, and 104 °C for the catalysts calcined at 450, 600, and 800 °C, respectively.

The reported data show that the catalyst calcined at 800 °C has the highest reaction rate at 25 °C; its rate is approximately ten-fold higher than the reaction rates of the samples calcined at 450 and 600 °C. The activation energies calculated from the slopes of the curves are 42–46 kJ/mol for all of the samples.

The 3.8%Pd/CeO_2 samples calcined at 450 and 800 °C also show diminution of the CO conversion at 80–110 °C. The 3.8%Pd/CeO_2-600 °C sample exhibits an S-shape behavior in the CO conversion curve, where the maximum of conversion is attained in a short time. For the catalysts calcined at 450, 600, and 800 °C, T_{10} is equal to 29, 8, and 29 °C, and T_{50} is 70, 33, and 70 °C, respectively. From these results, we find that the reaction rates calculated at 25 °C for the samples calcined at 600 and 800 °C are four-fold higher than those calculated for the sample calcined at 450 °C and that the activation energies for these samples fall in the range of 38–42 kJ/mol.

For the 7.7%Pd/CeO_2 samples, the T_{10} values are equal to 5, –1, and 25 °C, and the T_{50} values are 43, 17, and 62 °C after calcination at 450, 600, and 800 °C, respectively. The reaction rate calculated at 25 °C for the 7.7%Pd/CeO_2-600 °C sample is nearly two-fold higher compared with 7.7%Pd/CeO_2-450 °C and 1.5-fold higher compared with 7.7%Pd/CeO_2-800 °C. The activation energies for these samples are in the range of 25–42 kJ/mol.

Therefore, it can be concluded that the lowest values of T_{10} and T_{50}, indicating the highest catalytic activity in LTO CO, were obtained for the catalysts containing 7.7% Pd and for the 3.8%Pd/CeO_2-600 °C sample.

The data on the activity of the 0.74%Pd/CeO_2 catalyst show that increasing the calcination temperature from 450 to 600 °C does not change the reaction rate, while calcination at 800 °C results in a ten-fold increase in the reaction rate. For the 3.8%Pd/CeO_2 catalyst, the reaction rate increases four-fold as the calcination temperature is raised from 450 to 600 °C, whereas calcination at 800 °C provides no additional effect on the reaction rate. Finally, for the 7.7%Pd/CeO_2 catalyst, the sample calcined at 600 °C is the most active; however, the difference in activity among the three samples of this series is not substantial, and the difference in reaction rates for this catalyst is less than two-fold for the samples calcined at 450 and 800 °C. Thus, as follows from the data shown in Fig. 1, the calcination temperature is a critical parameter for the low-percentage palladium catalyst, whereas it is not as important at a high palladium content. For the latter, maximum activity can be attained using the relatively low calcination temperature of 600 °C.

Typical behavior of the dependence of the catalytic activity on palladium loading and calcination temperature can be observed in

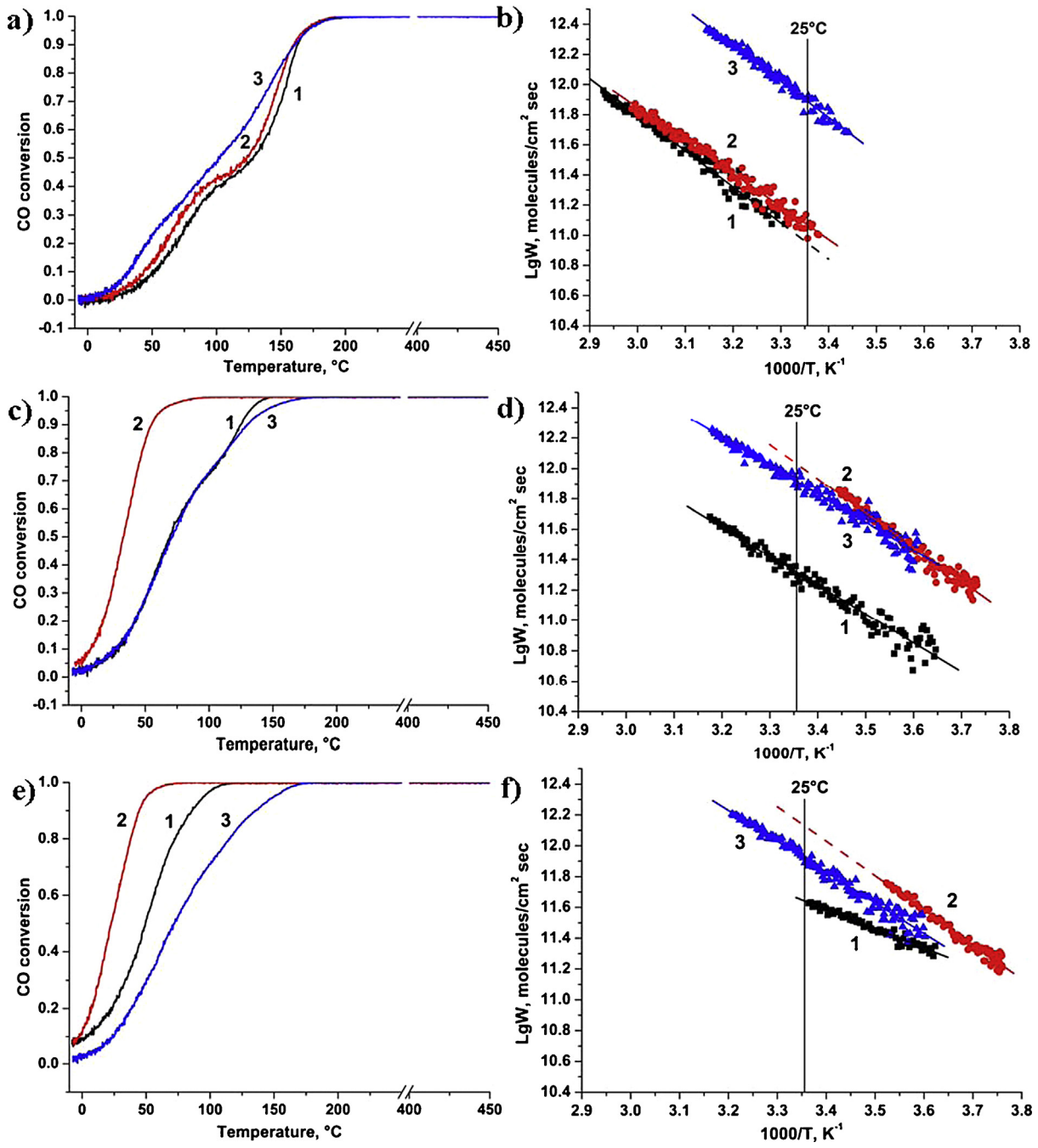

Fig. 1. Temperature dependences of CO conversion (a, c, e) and Arrhenius dependences of CO oxidation rate (b, d, f) for catalysts Pd/CeO_2 calcined at 450 °C (1), 600 °C (2) and 800 °C (3). The catalysts contained 0.74%Pd (a, b), 3.8%Pd (c, d), 7.7%Pd (e, f).

the plots of CO oxidation rate displayed in Fig. 2. For the samples calcined at 450 °C, the reaction rate on the catalyst increases by a factor of 2.2 and 4.6 when the palladium content is raised from 0.74 to 3.8 and 7.7%, respectively. For the samples calcined at 600 °C, the reaction rate increases by a factor of 9 and 11 as the palladium content is increased from 0.74 to 3.8 and 7.7%, respectively. For the samples calcined at 800 °C, the reaction rate is virtually identical for all palladium concentrations.

The results shown in Fig. 2 indicate that the loading of the active component plays quite an important role, but not for all calcination temperatures. Presumably, the data on the catalytic activity displayed in Figs. 1 and 2 indicate a strong structural modification of the sample surface and changes in both the concentration and the state of the active component.

3.2. XRD study

The main phase observed in the diffraction patterns is modified ceria (CeO_2) with a fluorite structure. Palladium oxide (PdO) as an individual phase is reliably detected only in the samples that have a high palladium content (7.7%). The low sensitivity of the method to this phase is related to the substantial width of the peaks and overlapping of the most intense PdO reflections with CeO_2 reflections. Fig. 3 displays a fragment of the diffraction pattern for the 7.7%Pd/CeO_2-800 °C sample with deconvolution of the total profile into components, which was generated by the Rietveld method.

As noted above, the observed reflections are characterized by a substantial physical broadening, which is caused by the small sizes of the crystallites (Table 1). The crystallite size in the CeO_2 phase is

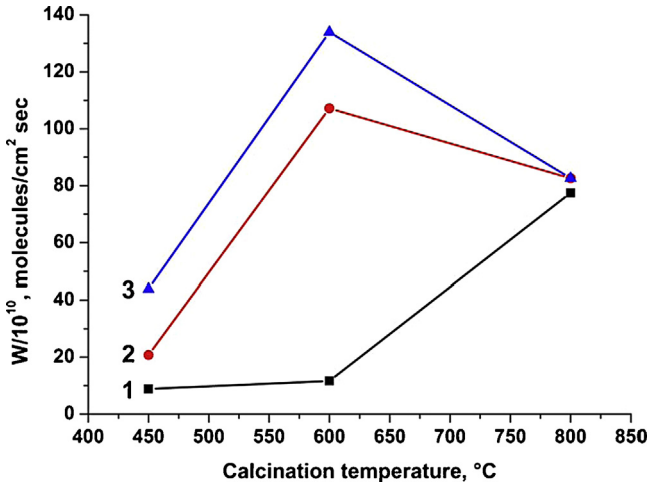

Fig. 2. Dependence of CO oxidation rate on the calcination temperature for catalysts Pd/CeO_2 contained 0.74% (1), 3.8% (2), 7.7% (3) Pd. CO oxidation rate was calculated for 25 °C.

somewhat smaller compared with that in the PdO phase. Of particular note is the strong effect of palladium oxide on the crystallinity of the ceria phase. The size of the CeO_2 crystallites in the 7.7%Pd/CeO_2-450 °C sample was measured to be 5.8 nm (Table 1), while in pure ceria synthesized under the same conditions, they are 10.4 nm. An increase in the calcination temperature leads to coarsening of the crystallites: the size of the crystallites in the samples calcined at 800 °C reaches 17–25 nm.

Refinement of the ceria lattice parameter results in insignificant (within the experimental error) deviations from the value reported in the literature (PDF card – 34-394).

3.3. XPS study

3.3.1. 0.74%Pd/CeO_2 catalyst

The composition of the catalysts surface was calculated using XPS data for all the studied samples and is presented in Table S1. Fig. 4 displays the Pd3d spectra for all of the catalysts, normalized against the Ce3d line. In this case, the intensity of Pd3d line represents, to a first approximation, the concentration of palladium in the surface layers of the catalyst. For the low-percentage 0.74%Pd/CeO_2 catalysts calcined at 450 and 600 °C, the Pd3d spectra exhibit low intensity, most likely due to the predominantly bulk location of the palladium. As observed from the Pd3d spectra (Fig. 4a, curves 1 and 2), the state of the palladium is uniform and exhibits a doublet at $E_b(Pd3d_{5/2}) = 338.0$ eV, corresponding to the solid solution $Pd_xCe_{1-x}O_{2-\delta}$ [3,11,23,25,33–38].

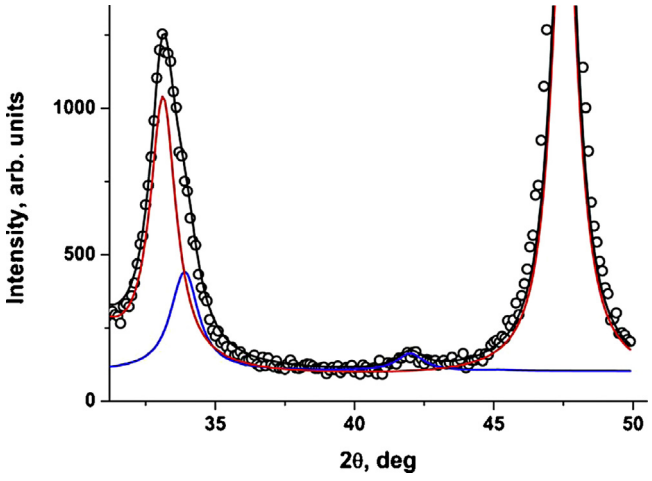

Fig. 3. Fragment of X-ray diffraction patterns for 7.7%Pd/CeO_2-800 °C catalyst with curves decomposition: circles – experimental points; calculated diffraction patterns: red line – CeO_2, blue line – PdO, black line – summary profile. (For interpretation of the references to color in this figure legend, the reader is referred to the web version of this article.)

Raising the calcination temperature of the catalyst to 800 °C strongly increases the total intensity of the Pd3d line, and a new additional state with binding energy $E_b(Pd3d_{5/2}) = 336.1$ eV appears in the spectrum (Fig. 4a, curve 3). The growth of Pd3d line intensity can be attributed to sintering of the ceria particles (Table 1) and the appearance of Pd^{2+} ions on the catalyst surface. The XPS data (Table 2) indicate that the surface of the 0.74%Pd/CeO_2 catalysts calcined at 450 and 600 °C have low palladium content, whereas calcination at 800 °C leads to a considerable enrichment of the surface with palladium. In the process, the palladium concentration on the surface exceeds 2.5-fold its concentration, as determined by chemical analysis. This result suggests that calcination at 800 °C stimulates both an increase in the subsurface concentration of Pd^{2+} ions in the solid solution of $Pd_xCe_{1-x}O_{2-\delta}$ with $E_b(Pd3d_{5/2}) = 338.0$ eV and the release of palladium to the surface with the formation of the "oxide-like" structures with $E_b(Pd3d_{5/2}) = 336.1$ eV. Considering that the binding energy of the additional peak (336.1 eV) in the spectrum differs from the value typical of PdO ($E_b(Pd3d_{5/2}) = 336.7–337.1$ eV) [39–41], we find that a release of palladium to the surface in the form of PdO nanoparticles does not occur.

This result suggests that on the surface of the solid solution of $Pd_xCe_{1-x}O_{2-\delta}$ enriched with palladium, either the two-dimensional PdO_x(s) structures or the oxidized Pd–O–Ce(s) surface species are formed, which contain a much greater fraction of palladium compared with the palladium content in the bulk of the solid solution. The presence of the oxidized palladium species on the surface of the $Pd_xCe_{1-x}O_{2-\delta}$ solid solutions has been noted elsewhere [42,43]; however, photoelectron spectroscopy was not employed in those works, and information on the position of the Pd3d level in these structures was not reported. Nevertheless, the presence of a certain amount of palladium oxide nanoparticles cannot be ruled out in this case because a weak signal in the Pd3d spectrum with a binding energy close to 337 eV may be masked by the more intense signals with $E_b = 336.1$ and 338.0 eV.

3.3.2. 3.8%Pd/CeO_2 catalyst

The 3.8%Pd/CeO_2 catalyst calcined at 450 °C is characterized by an expectedly more intense Pd3d line with $E_b(Pd3d_{5/2}) = 338.0$ eV, which corresponds to the substitution solid solution $Pd_xCe_{1-x}O_{2-\delta}$. In addition to this state, a low-intensity peak with $E_b(Pd3d_{5/2}) = 336.5$ eV is observed (Fig. 4b, curve 1). This binding energy is somewhat lower than the value that is typical of the bulk (extended) PdO; therefore, in this case, the peak can be attributed to small PdO particles according to [44]. We believe that the increased palladium content in the initial solution is why palladium cannot be incorporated completely into the CeO_2 lattice at coprecipitation during the synthesis. Therefore, a portion of the palladium can form the PdO nanoparticles. Calcination of the catalyst at 600 °C (the 3.8%Pd/CeO_2-600 °C sample), in contrast to the 0.74%Pd/CeO_2-600 °C catalyst, increases the intensity of the Pd3d line (Fig. 4b, curves 1 and 2). In this case, the release of Pd^{2+} ions to the surface of the CeO_2 particles becomes noticeable at 600 °C, most likely due to a greater amount of the initial PdO nanoparticles. Nevertheless, the catalyst surface still has low palladium content as a result of the relatively low calcination temperature, 600 °C.

Similar to the 0.74%Pd/CeO_2-800 °C catalyst, the appearance of an additional doublet with $E_b(Pd3d_{5/2}) = 336.2$ eV (Fig. 4b, curve 2) should also be noted in this case, which indicates the formation of

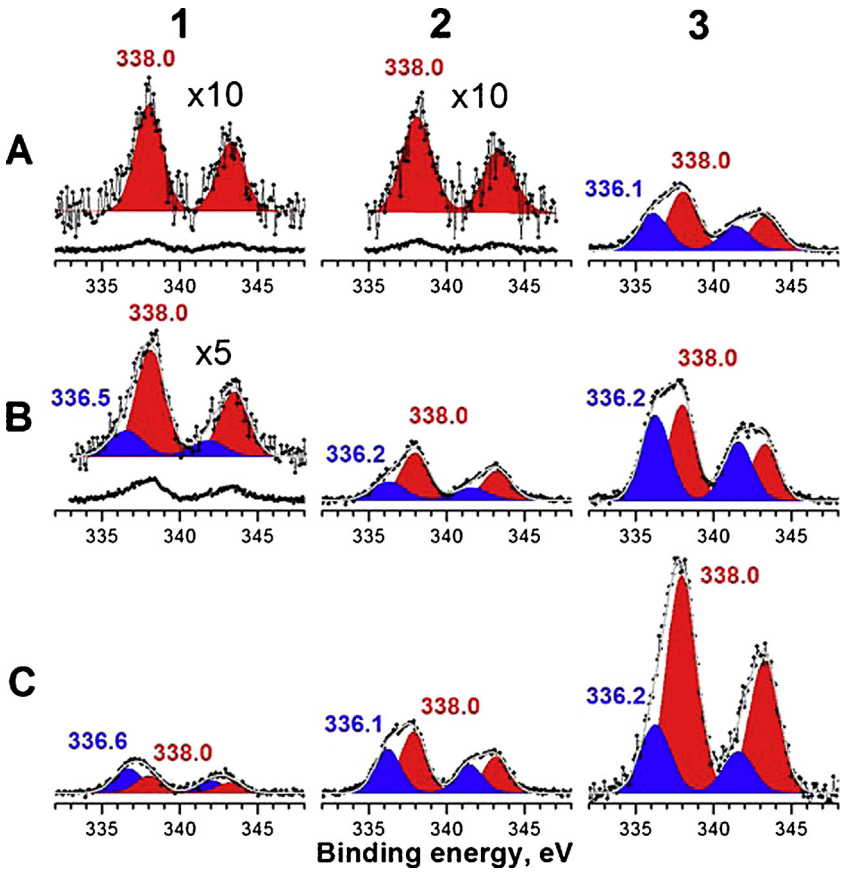

Fig. 4. Pd3d spectra, normalized to the integrated intensity of Ce3d line, obtained for the catalysts 0.74%Pd/CeO_2 (A), 3.8%Pd/CeO_2 (B) and 7.7%Pd/CeO_2 (C) calcined at 450 °C (1), 600 °C (2) and 800 °C (3).

PdO_x(s)/Pd–O–Ce(s) structures that differ from those of PdO oxide. Calcination of the 3.8%Pd/CeO_2 catalyst at 800 °C produces a further increase in the intensity of the Pd3d line due to both the component with $E_b(Pd3d_{5/2})$ = 338.0 eV and an even more sharp growth of the component with $E_b(Pd3d_{5/2})$ = 336.2 eV. As a result, the intensities of the peaks corresponding to both states become approximately equal. Although palladium is present as two species with the surface and bulk location, on average, the palladium concentration on the surface corresponds to the mean analytical value (Table 2).

3.3.3. 7.7%Pd/CeO_2 catalyst

On the surface of the 7.7%Pd/CeO_2 catalyst calcined at 450 °C, palladium is present in two states: as the solid solution $Pd_xCe_{1-x}O_{2-\delta}$ ($E_b(Pd3d_{5/2})$ = 338.0 eV) and as PdO oxide ($E_b(Pd3d_{5/2})$ = 336.6 eV) (Fig. 4c, curve 1). Of the two forms, the fraction of palladium contained in the PdO nanoparticles is greater, which may be related to the efficient formation of palladium oxide nanoparticles at high concentrations of palladium in the solution during coprecipitation. The formation of PdO nanoparticles was confirmed by the XRD data (Fig. 3, Table 1).

Calcination of this catalyst at 600 °C increases the total intensity of Pd3d line, similar to the catalysts with lower palladium content. As in the case of the 3.8%Pd/CeO_2-600 °C catalyst, the disappearance of the $E_b(Pd3d_{5/2})$ = 336.6 eV peak and the appearance of a peak with $E_b(Pd3d_{5/2})$ = 336.1 eV are observed, which results from a partial transition of the PdO nanoparticles to the interaction state with the ceria surface to form the PdO_x(s)/Pd–O–Ce(s) structures. According to the XRD data, not all of the PdO particles are transformed into the two-dimensional structures in this case; therefore, the remaining fraction of PdO oxide, which is characterized by a signal with $E_b(Pd3d_{5/2})$ ~ 337.0 eV, is likely masked by the signals from palladium species with binding energies of 338.0 and 336.1 eV.

Calcination of the catalyst at 800 °C produces a sharp increase in the intensity of the Pd3d line, primarily due to a pronounced growth of the intensity of a component at 338.0 eV, corresponding to the solid solution. It can be expected that along with crystallization and the increasing particle sizes of the ceria and PdO (Table 2), there occurs a further dissolution of the residual PdO in the bulk of ceria with the increase of its concentration in the subsurface layers.

Fig. 5 displays the dependencies of the surface concentration of palladium, as measured by XPS, on the calcination temperature and palladium loading in the catalyst. One can see from Fig. 5a that the surface concentration of palladium in the catalyst containing 0.74%Pd does not change upon calcination at 450 and 600 °C,

Table 2
The total surface concentration of palladium with respect to cerium (Pd_{atom}/Ce_{atom}, %) depending on the content of palladium and calcination temperature of catalysts.

Pd/Ce, mol.%	T_{calc}, °C	0.74 wt.% Pd/CeO_2 1.19 mol.%Pd/CeO_2 Pd/Ce = 1.2	3.8 wt.% Pd/CeO_2 6.0 mol.%Pd/CeO_2 Pd/Ce = 6.4	7.7 wt.% Pd/CeO_2 11.9 mol.%Pd/CeO_2 Pd/Ce = 13.5
	450	0.29	0.76	1.38
	600	0.3	2.11	3.04
	800	2.98	6.23	9.43

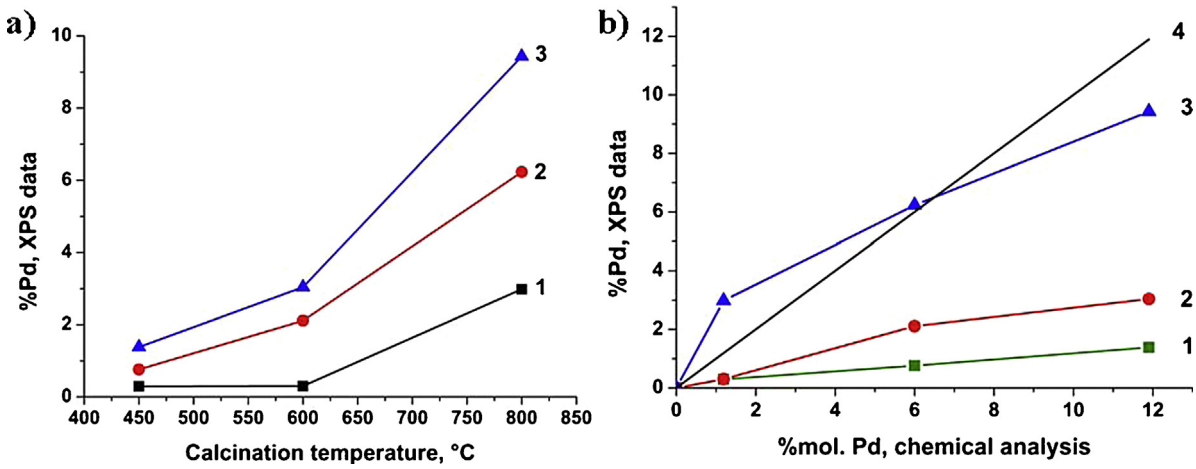

Fig. 5. Pd surface concentration calculated from XPS data depending on: (a) the calcination temperature for samples with Pd loading 0.74% Pd (1), 3.8%Pd (2), 7.7%Pd (3); (b) total loading of palladium for samples with different calcination temperatures: 450 °C (1), 600 °C (2), 800 °C (3). Curve 4 – line which corresponds to the same concentration of palladium in the bulk and on the surface of samples. Values above and below line 4 indicate the surface enrichment and depletion of palladium, respectively.

whereas calcination at 800 °C leads to its growth. For the samples containing 3.8 and 7.7%Pd, the surface concentration of palladium increases during the calcination at 600 °C and shows a sharp growth upon calcination at 800 °C. Fig. 5b reflects the dependence of the surface palladium concentration on its loading in the catalysts calcined at different temperatures, which is revealed by the chemical analysis. As observed from the reported data, the surface palladium concentration for the catalysts calcined at 450 and 600 °C is below the value corresponding to equal concentrations in the bulk and on the surface. This finding affirms that in these samples, the surface is depleted with palladium compared with the bulk. For the catalysts calcined at 800 °C a different behavior is observed. For the catalyst containing 0.74%Pd, the surface concentration of palladium is higher than in the bulk, which indicates the enrichment of the surface with palladium. For the catalyst containing 3.8%Pd, the surface palladium concentration is equal to that in the bulk, which indicates a uniform distribution of palladium over the surface and in the bulk. Finally, for the catalyst containing 7.7%Pd, the surface palladium concentration is lower than the bulk, which indicates that the surface is depleted with palladium compared with the bulk.

3.4. HRTEM study

As shown by HRTEM, three-dimensional palladium structures are not observed in the samples with low palladium content (0.74%). Nevertheless, the low-intensity PdL signal is present in the EDX spectra of the support particles, which points to the stabilization of the palladium in the highly dispersed state. The presence of a small number of PdO nanoparticles is possible; however, such particles cannot be detected due to the low palladium content and high contrast of the CeO_2 support in the electron microscopy images.

Increasing the palladium content and calcination temperature leads to the formation of three-dimensional palladium structures, which were identified using EDX spectroscopy.

At a high calcination temperature (800 °C), the support in the 3.8%Pd/CeO_2-800 °C sample (Fig. 6) is represented by aggregates of CeO_2 nanoparticles with a size of 20–40 nm (Fig. 6a, region 1) and the flat porous CeO_2 plates with a length of up to 1 μm (Fig. 6a, region 2). A flat CeO_2 particle oriented toward the viewer at its smaller side is shown in Fig. 6a (region 2). TEM and HAADF-STEM images of the flat CeO_2 particles in a different orientation are presented in Fig. 6b and f. Fig. 6c and d depicts the SAED (Selected Area Electron Diffraction) patterns obtained from an aggregate of CeO_2 particles (Fig. 6a, region 1) and from a flat CeO_2 particle (Fig. 6b), respectively. The SAED pattern from the aggregate of CeO_2 particles has a circular shape due to merging of the single-type reflections from chaotically oriented CeO_2 nanoparticles. Bright point reflections are observed in the SAED pattern from a flat particle, which indicates that the observed plate-like particles are mesocrystals. In the high-resolution images, flattened nanoparticles 1–2 nm in size, which are likely to be clusters of PdO_x, are detected on the surface of CeO_2 particles (Fig. 6e) [25,33]. The small particles with the size less than 2 nm having flattened shape were observed on the surface of Pd/CeO_2 catalysts in our previous works [25,37]. The lattice fringes of these particles cannot be usually seen in HRTEM images due to disordering at the atomic level or rearrangement of the structure which is typical for small clusters [45]. In some cases HRTEM imaging can allow us detecting the interplanar distances corresponding to metallic palladium [25], but small oxidized particles are highly reactive and can be easily reduced under the action of electron beam, so we cannot distinguish them basing only on the HRTEM observation results.

The EDX mapping image (Fig. 6g) obtained from the sample patch displayed in Fig. 6f demonstrates that palladium is distributed over the entire support, particularly over the large plate-like particles; however, the relative amount of palladium is higher in the aggregates of CeO_2 particles. The EDX mapping image (Fig. 6i) obtained at a greater magnification from the sample patch displayed in the HAADF-STEM image (Fig. 6h) makes it possible to detect local nonuniformities in the palladium distribution over the sample. Fig. 6i shows the accumulated signal in a small section at the bottom of the image, which can be attributed to the formation of palladium nanoparticles in the CeO_2 agglomerates.

A non-uniform distribution of palladium is observed in the 7.7%Pd/CeO_2 samples with increased palladium content. Thus, in the 7.7%Pd/CeO_2-600 °C sample (Fig. 7), aggregates with a size of ca. 50–130 nm, which consist of PdO and CeO_2 particles, are formed (Fig. 7a). Such aggregates have an increased contrast in the electron microscopy images compared with the CeO_2 particles. Fig. 7b displays the EDX spectrum from an aggregate of PdO–CeO_2 particles, which demonstrates a high intensity of the PdL line. The EDX spectrum of the support particles that are free of PdO (Fig. 7c) has a low-intensity peak of PdL, which is attributed to the presence of palladium in a highly dispersed state (clusters or ionic species). Analysis of HRTEM images of the aggregates having intense PdL line in EDX spectra allowed us to detect crystallites with the size of about 5 nm with interplanar distances corresponding to PdO phase. One of such particles is seen in Fig. 7d aligned along the [0 0 1]

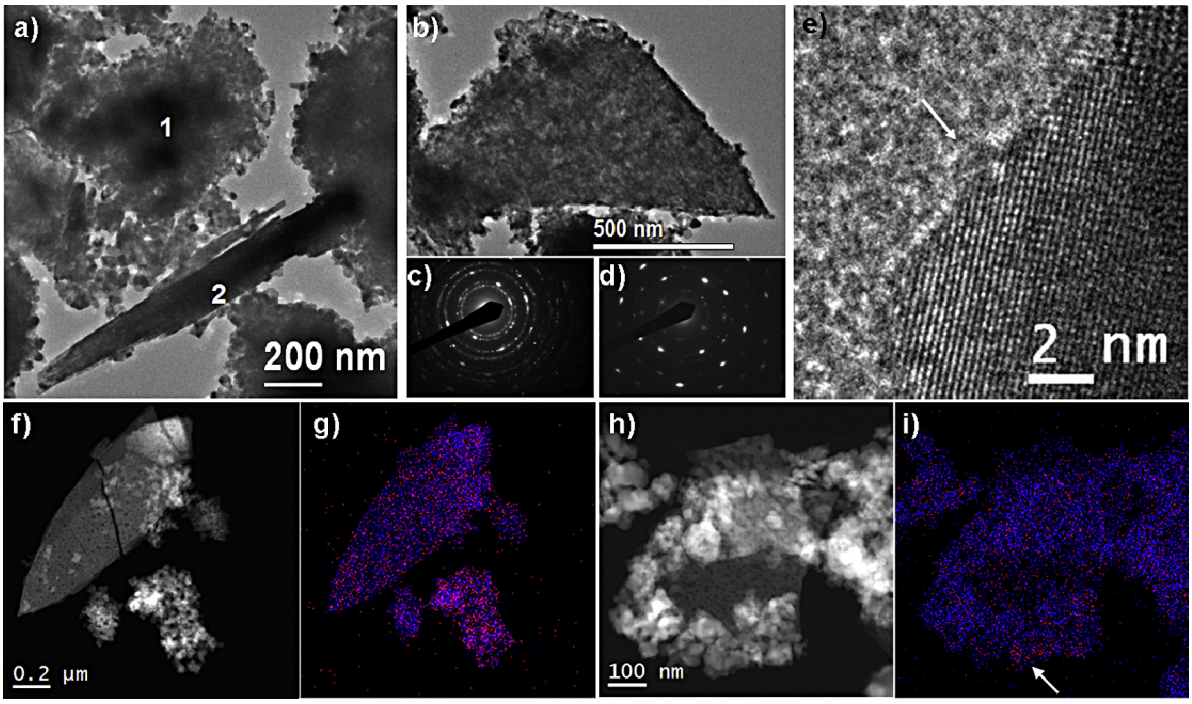

Fig. 6. (a) TEM-image of the 3.8%Pd/CeO_2-800 °C catalyst: aggregate of spherical CeO_2 nanoparticles (1) and flat CeO_2 nanoparticles (1), (b) HRTEM-image of the flat CeO_2 particle in different orientation; (c, d) SAED patterns obtained from an aggregate of CeO_2 particles ((a), region 1) and from a flat CeO_2 particle (b), respectively; (e) HRTEM-image of the PdO_x nanoparticle on the CeO_2 surface; (f–i) HAADF-STEM images and corresponding EDX-mapping patterns (CeL signal is shown in blue, PdL signal is shown in red). (For interpretation of the references to color in this figure legend, the reader is referred to the web version of this article.)

direction. The inset shows the corresponding FFT pattern from this particle where reflections from PdO phase are indicated. Fig. 7e and f displays the HAADF-STEM image of the sample section and its EDX mapping, which reveals the distribution of PdO nanoparticles in the bulk of the sample. Fig. 7g depicts the HAADF-STEM image obtained at greater magnification. The EDX mapping obtained from this section (Fig. 7h) allowed us to determine that PdO particles are located primarily "inside" the aggregates and are covered with CeO_2 nanoparticles. The size of the CeO_2 particles is ca. 4–5 nm, while the size of the PdO particles does not exceed 15 nm. As it can be seen from Fig. 7g and h some of the PdO particles are located close to the edge of agglomerates and only one layer of CeO_2 nanoparticles (about 5 nm width) covers them. The intensity of Ce L signal in EDX-maps of these areas is quite lower comparing to the signal from the center of agglomerates. This makes it difficult to see these CeO_2 particles in the EDX-mapping image, while they still can be seen in HAADF-STEM image. Also we should mention that we can see only one two-dimensional projection of the particle agglomerate so we cannot be sure that the definite PdO particle is not located on the edge of agglomerate in other projection. But, observation of different sample areas in HRTEM mode and in EDX-mapping mode did not allow us to detect any PdO particles on the edge of agglomerate. So the conclusion about the location of PdO particles is based on statistical observation of different sample areas. As in the case of the 3.8%Pd/CeO_2-800 °C sample, PdO_x clusters with a size of ca. 1 nm are present on the support surface in the 7.7%Pd/CeO_2-600 °C sample (Fig. 7i).

Increasing the calcination temperature to 800 °C (sample 7.7%Pd/CeO_2-800 °C) results in the formation of an extended PdO phase. Fig. S1 displays the HAADF image and EDX mapping for one of the aggregates in the 7.7%Pd/CeO_2-800 °C catalyst. One can clearly see from these images that some of the palladium is concentrated more densely in certain sections of the catalyst. This may be related to the formation of a fraction of the palladium as large PdO particles, in accordance with the XRD data.

3.5. TPR-CO study

Investigation of the catalysts by the TPR-CO method in the absence of gas-phase oxygen allowed us to examine the reactivity of the catalyst oxygen toward carbon monoxide and to elucidate the main species. Fig. 8 shows the CO consumption and CO_2 evolution spectra during the temperature-programmed reaction with CO (TPR-CO) for all the initial samples. In the course of TPR-CO, CO_2 evolution is accompanied by a release of a certain amount of hydrogen and water (not shown in the figure).

The reported data indicate that the CO consumption spectra have four temperature ranges: −10 to 80 °C, 80 to 210 °C, 210 to 375 °C and above 375 °C.

At temperatures above 375 °C the profiles of CO consumption and CO_2 evolution coincide. According to the data reported in [46], it can be suggested that at these temperatures oxygen starts to diffuse from the bulk of support to the surface and interacts with the gas-phase CO. This is accompanied by the release of H_2. As shown in [47], hydrogen and carbon dioxide can be formed in the TPR-CO process due to the water–gas shift (WGS) caused by CO interaction with the hydroxyl groups on the catalyst surface: $CO(ads) + 2OH^-(support) \rightarrow CO_2(g) + H_2(g) + O^{2-}(support)$.

In the temperature range of 80–375 °C, the profiles of CO consumption and CO_2 evolution also virtually coincide and correspond to CO interaction with the active oxygen that was formed during the synthesis of Pd–ceria catalyst. All the TPR-CO curves for this temperature range are characterized by two peaks of CO consumption and CO_2 evolution with $T_{max} \sim 130$–180 °C (peak 2) and 270–320 °C (peak 3).

According to the previously obtained data [25], peak 2 corresponds to the reduction of PdO phase, while peak 3 is assigned to the reduction of $Pd_xCe_{1-x}O_{2-\delta}$ solid solution. These results agree well with the XRD and TEM data demonstrating the presence of PdO particles, whose size increases with the calcination temperature.

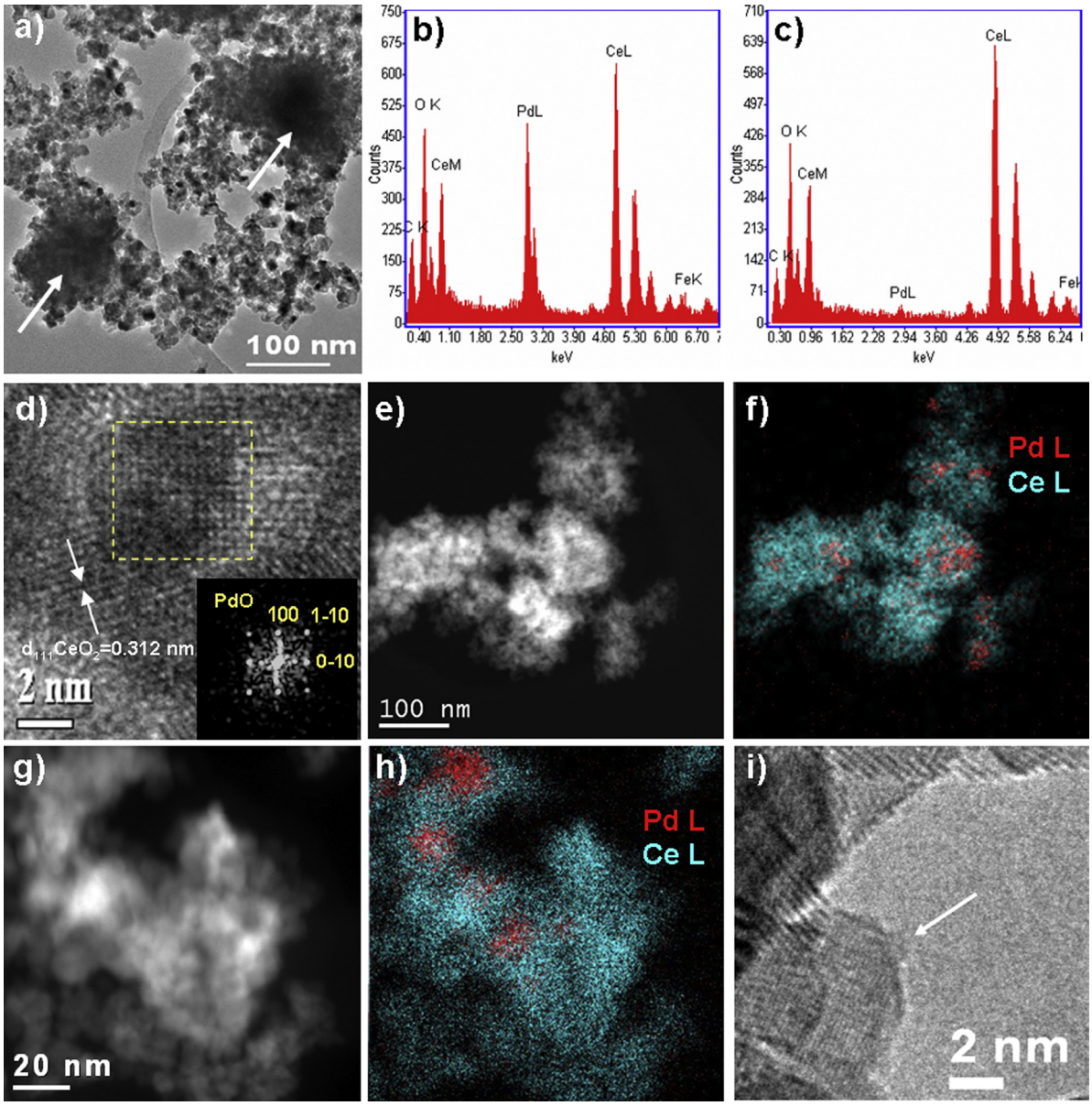

Fig. 7. TEM study of the 7.7%Pd/CeO_2-600 °C catalyst: (a) TEM-image showing aggregates of PdO and CeO_2 particles, (b) EDX spectrum from an aggregate of PdO–CeO_2 particles, (c) EDX spectrum from the support particles free of PdO, (d) HRTEM-image of CeO_2 and PdO nanoparticles in PdO–CeO_2 aggregate, the inset shows the FFT pattern of selected region with indication of PdO reflections (zone axis [0 0 1]); (e–h) HAADF-STEM images and corresponding EDX-mapping patterns (CeL signal is shown in cyan, PdL signal is shown in red); (i) HRTEM-image of the PdO_x nanoparticle on the CeO_2 surface. (For interpretation of the references to color in this figure legend, the reader is referred to the web version of this article.)

The behavior of peak 2 is quite sensitive to the initial concentration of palladium and the calcination temperature. As the calcination temperature raises, the area of this peak decreases. This was clearly demonstrated for the 3.8%Pd/CeO_2 catalyst, indicating a decrease in the amount of PdO phase due to dissolution of PdO nanoparticles. At the same time the area of peak 3 increases, i.e., the $Pd_xCe_{1-x}O_{2-\delta}$ solid solution is formed. It seems interesting that peak 2 is observed for the 0.74%Pd/CeO_2 catalyst only after its calcination at 450 °C, whereas raising the calcination temperature to 600 °C results in lowering of peak 2, which completely disappears from CO consumption spectra after increasing the calcination temperature to 800 °C.

Along with the typical behavior of peaks 2 and 3, an additional substantial feature appeared in the TPR-CO spectra: a discrepancy between the profiles of CO consumption and CO_2 evolution in the temperature range from −10 to 80 °C. Thus, for all the samples displayed in Fig. 8, CO consumption starts already at negative temperatures and reaches a maximum at ~50 °C (peak 1), while CO_2 evolution starts much later: at 70 °C, 30 °C and −10 °C for the 7.7%Pd/CeO_2 catalysts calcined at 450 °C, 600 °C and 800 °C, respectively. Thus, peak 1 in the CO_2 evolution spectra of 7.7%Pd/CeO_2 catalyst manifests itself as: (1) a low-temperature shoulder of peak 2 for the 7.7%Pd/CeO_2-450 °C catalyst, (2) an unresolved peak with a maximum near 75 °C for the 7.7%Pd/CeO_2-600 °C catalyst, and (3) a single peak with a maximum near 55 °C for 7.7%Pd/CeO_2-800 °C. It is noteworthy that though the most weakly bound state is formed in the 7.7%Pd/CeO_2 catalyst after calcination at 800 °C, the highest concentration of this state is observed in the sample after its calcination at 600 °C. A similar behavior was observed for the catalysts with palladium content of 3.8% and 0.74% (Fig. 8c–f).

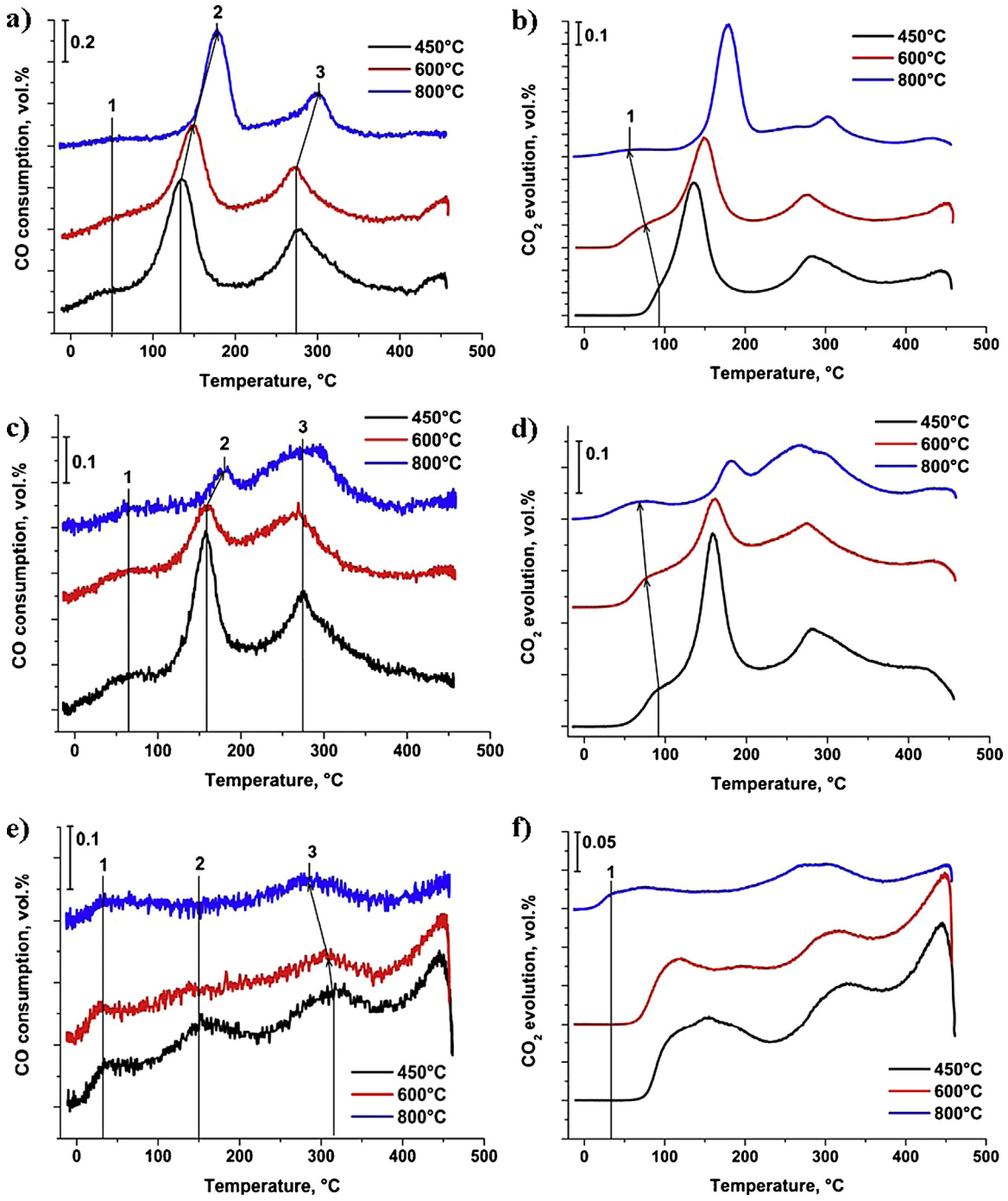

Fig. 8. The temperature dependences of the CO consumption (a, c, e) and CO_2 evolution (b, d, f) during the TPR-CO for the catalysts 7.7%Pd/CeO_2 (a, b), 3.8%Pd/CeO_2 (c, d), 0.74%Pd/CeO_2 (e, f) calcined at 450, 600 and 800 °C.

The data obtained in our study demonstrate that in the low-temperature region an unusual state of palladium exists. This state differs from the PdO phase and from Pd^{2+} inside of $Pd_xCe_{1-x}O_{2-\delta}$ solid solution and can be related to the surface clusters PdO_x(s)/Pd–Ce–O(s), where $x < 1$. The indicated state is active at low temperatures and has $E_b(Pd3d_{5/2}) = 336.1$ eV in XPS spectra.

Thus, the TPR-CO spectra displayed in Fig. 8 show that the Pd/CeO_2 catalysts synthesized by coprecipitation have three types of active species associated with the presence of palladium in the catalysts. The PdO and $Pd_xCe_{1-x}O_{2-\delta}$ phases have been identified in our previous studies, while in these experiments we have managed to reveal for the first time the most weakly bound state of oxygen, which may be related either to its location on the surface as flattened PdO_x(s) clusters (2D structures) or to the formation of surface mixed oxide Pd–Ce–O(s) species, whose nature is unclear now.

4. Discussion

4.1. Pd species in Pd/CeO_2 catalysts

The results obtained for the catalysts synthesized by coprecipitation demonstrate that a fraction of palladium dissolves in CeO_2 with formation of the solid solution $Pd_xCe_{1-x}O_{2-\delta}$, and the

remaining palladium is present as PdO nanoparticles. The interaction between PdO and $CeO_2/Pd_xCe_{1-x}O_{2-\delta}$ particles makes PdO nanoparticles to serve as the seeds for the aggregation of ceria around PdO particles. The formation of PdO-ceria aggregates was shown by TEM and EDX-mapping data and was confirmed by the quantitative analysis of XPS data showing less surface concentration of palladium comparing to the bulk content. The distribution of palladium between PdO and $Pd_xCe_{1-x}O_{2-\delta}$ phases depends on Pd loading and the calcination temperature. The obtained data showed that the greater relative proportion of palladium in oxide phase PdO was formed in the catalysts with higher palladium loading. TPR-CO results show reliably the dissolution of PdO phase inside the ceria lattice at increasing the calcination temperature. This dissolution occurs due to the strong interaction between palladium and ceria with formation of stable $Pd_xCe_{1-x}O_{2-\delta}$ solid solution. Such interaction is proposed to be realized at the particles interface with dissolution of a part of PdO within the fluorite phase. This leads to enrichment of the surface-subsurface layers of ceria with palladium ions Pd^{2+} and was observed in XPS spectra as an increase in the intensity of Pd3d doublet with $E_b(Pd3d_{5/2}) = \sim 338.0$ eV. This dissolution of PdO is an additional source for increasing the content of Pd^{2+} ions in the cerium oxide lattice, which stimulates the segregation process upon rise of the calcination temperature.

TPR-CO (Fig. 8) and XPS (Fig. 4) data showed the presence of definite peaks (peak 1 in TPR-CO and $E_b(Pd3d_{5/2}) = \sim 336.1$ eV in XPS spectra), which suggest the formation of oxidized palladium structures $PdO_x(s)/Pd–O–Ce(s)$ on the surface of $Pd_xCe_{1-x}O_{2-\delta}$ particles. The presence of such structures is also confirmed by TEM data showing highly dispersed palladium particles on the ceria surface (Figs. 6e and 7i). These surface compounds appear as a result of the direct interaction of PdO particles with the surface of CeO_2 or $Pd_xCe_{1-x}O_{2-\delta}$ particles, or due to diffusion of Pd^{2+} ions to the surface of the solid solution $Pd_xCe_{1-x}O_{2-\delta}$, with the subsequent release of the excess palladium from the solid solution to the support surface. The surface species contain a greater fraction of palladium compared with the solid solution because the surface layers of the support are being enriched with palladium during the calcination, as observed from the Pd/Ce ratio in XPS spectra.

Increase of the calcination temperature leads to coarsening and sintering of both PdO and CeO_2 particles, as shown by XRD and HRTEM. The XPS data indicate that palladium is present both as Pd^{2+} in $Pd_xCe_{1-x}O_{2-\delta}$ and as small oxidized clusters of $PdO_x(s)/Pd–O–Ce(s)$ with $E_b(Pd3d_{5/2}) = \sim 336.1$ eV. Note that the value $E_b(Pd3d_{5/2}) = \sim 336.1$ eV is quite low in comparison with binding energy value for PdO oxide. This state of palladium cannot be attributed to the PdO phase, which is present in the catalysts with high palladium content. In addition, the Pd/CeO_2 catalysts containing only the PdO phase and cerium oxide phase are inactive toward the oxidation of CO at temperatures below 150 °C [25].

The XPS data indicate a considerable subsurface enrichment of the fluorite phase with palladium ions in the catalysts calcined at 800 °C. Naturally, such enrichment increase the concentration of Pd^{2+} ions referred to the unit surface of $Pd_xCe_{1-x}O_{2-\delta}$ solid solution. It means that the cationic sublattice on the surface of solid solution particles will be strongly distorted, since Pd^{2+} ions are shifted with respect to the fluorite position in CeO_2 [37]. Such distortions will facilitate the output of palladium ions to the surface with the formation of more stable surface structures. On the other hand, relative closeness of palladium ions to each other on the surface of fluorite phase will promote their aggregation into clusters upon reduction. It is supposed that such clusters may be formed on the surface of subsurface-enriched palladium solid solution even under UHV conditions when taking the XPS spectra. We think that such clusters are very small and comprise several palladium atoms.

Thus, small palladium cluster anchored on the solid solution surface contain a limited number of Pd–Pd bonds comparable with the number of Pd–O bonds. From this standpoint, the notion of stoichiometric composition of these species loses its sense; so, we denote this state as PdO_x clusters, implying that $x < 1$, and the oxidation state has a value intermediate between Pd^0 and Pd^{2+}, formally close to 1+. Accordingly, the intermediate oxidation state gives a shift of the Pd3d doublet toward low binding energies approximately by 1 eV. It should be noted that a decrease in the size of the PdO clusters produces some decrease in the binding energy of Pd3d to $E_b(Pd3d_{5/2}) = 336.5$ eV, which was noted in our earlier work [44]. It was also reported in our previous work [48] that $E_b(Pd3d_{5/2})$ for oxygen in 2D palladium oxide structures is by ~0.5 eV lower than in the bulk PdO. So, the binding energies values reduced by ~0.5–1.0 eV are quite expected for the surface palladium oxide structures.

4.2. Correlation of the catalytic activity and catalyst structure

The data obtained from the discussed physical measurements (Figs. 3–8) along with the catalytic data displayed in Figs. 1, 2 and 8 can be used to make certain conclusions about the palladium and palladium–cerium structures that determine the activity of the catalysts for the low-temperature oxidation of CO.

As observed from Fig. 1a, the $0.74\%Pd/CeO_2$ catalysts with a low palladium loading have some low-temperature activity, but their characteristics (the ignition temperature, the temperature of attaining 50% and 100% conversions) do not allow these catalysts, irrespective of the calcination temperature, to be considered an efficient catalytic system. Evidently, the observed moderate activity in LTO CO is related to the low palladium loading and low concentration of active sites on the surface. Indeed, as noted above, at a low palladium loading and low calcination temperatures of 450 and 600 °C, palladium is located predominantly in the bulk of the nanoparticle agglomerates and the remaining fraction of palladium resides directly in the bulk of ceria nanoparticles as the substitution solution $Pd_xCe_{1-x}O_{2-\delta}$. Therefore, the concentration of active sites determined by the presence of palladium on the surface is negligible in this case. The low concentration of active sites results in the S-shaped behavior of the light-off curves shown in Fig. 1a. The first (initial) part of the light-off curves in the range of 20–120 °C is determined by the active sites involving palladium, while the second part of the light-off curves starting from 120 °C and moving toward higher temperatures is related most likely to the catalytic action of PdO nanoparticles in the catalyst without the involvement of ceria [49]. The accessibility of PdO nanoparticles to the reaction medium is due to the presence of CeO_2 micropores covering the PdO particles. At temperatures above 200 °C, the particles of CeO_2 support also become catalytically active [12,50]. Their contribution to the total rate of the reaction at high temperatures cannot be excluded, but it is impossible to measure such particles because 100% conversion is attained in all cases at a lower temperature.

Increasing the calcination temperature of the low-percentage catalyst to 800 °C produces a substantial increase in the specific rate of the reaction (Fig. 2, curves 1–3). Therewith, the XPS data reveal the appearance of the oxidized $PdO_x(s)/Pd–O–Ce(s)$ structures on the surface of the bulk $Pd_xCe_{1-x}O_{2-\delta}$ phase, which means that the number of active surface sites in the catalyst increases. However, the temperature dependence of CO conversion shifts only slightly toward low temperatures (Fig. 1a, curve 3). The most likely reason is that the total amount of surface active sites sharply drops due to a decrease in the surface area as a result of catalyst sintering. The sharp decrease in the surface area of the support after calcination at 800°, which occurs also in the catalysts with increased palladium content, accounts for the shift of the light-off curves toward higher temperatures, as revealed by catalytic testing (Fig. 1c and e). Calcination at 800 °C stimulates a release of palladium to the external surface of the support nanoparticles, thereby increasing

the concentration of active sites and the catalytic activity. Nevertheless, the effect of crystallization and coarsening of the ceria particle size, which decreases the number of active sites, prevails for the high-percentage catalysts (Fig. 2).

As observed from Figs. 1 and 2, the catalysts possessing the highest activity and providing the best characteristics for LTO CO are 3.8Pd/CeO_2-600 °C and 7.7Pd/CeO_2-600 °C, i.e., the catalysts with increased palladium content. One can see that increasing the palladium content and increasing the calcination temperature to 600 °C leads to an increase in the reaction rate of CO oxidation referred to 1 cm^2 of the surface. The curve of CO conversion shifts to lower temperatures and a 100% conversion of CO is attained rapidly. Such behavior can be attributed to both the increase in the number of active surface sites in the catalyst calcined at 600 °C and to the retention of the highly dispersed structure of the support, which provides the total amount of such active sites. Overall, these factors provide the best catalytic performance.

Thus, PdO_x(s)/Pd–O–Ce(s) and $Pd_xCe_{1-x}O_{2-\delta}$ species both are responsible for low-temperature activity. The state of PdO_x cannot be considered separately from the solid solution because it is the product of Pd^{2+} ions segregation to the surface of fluorite phase. It should be noted that the appearance of such states of palladium correlates both with the catalytic activity toward the CO + O_2 reaction and with the general behavior of TPR-CO curves. In the case of samples calcined at 800 °C, the CO consumption and CO_2 evolution start simultaneously at a temperature near −10°C, whereas in the catalysts calcined at lower temperatures the CO_2 evolution starts at a much higher temperature. The initial section of TPR curves for CO_2 evolution can be attributed exactly to CO interaction with the surface PdO_x(s)/Pd–Ce–O(s) clusters, which are directly accessible for the CO adsorption. As follows from TPR-CO data, such $PdO_x/Pd_xCe_{1-x}O_{2-\delta}$ complex is catalytically active below room temperature. It cannot be ruled out that such clusters are efficiently formed in the course of CO + O_2 reaction (due to the presence of CO as a reducing agent) and can serve as the sites for activation of CO molecules. In our opinion, this peculiarity of PdO_x clusters can interrelate the catalytic activity in the low-temperature oxidation and the concentration of the indicated palladium species on the surface.

5. Conclusions

Using the coprecipitation method Pd/CeO_2 catalysts were synthesized with a range of palladium loading (0.74–7.7 wt.%) and calcination temperatures (450–800 °C). The application of XRD, TEM, XPS and TPR-CO allowed us to study the formation of the various components of the catalysts in different morphological and structural forms and correlate them with the catalytic activity.

It was shown that the coprecipitation synthesis and subsequent calcination at 450 °C results in the formation of two main types of the catalysts components: PdO (E_b(Pd3$d_{5/2}$) = 336.5 eV) and CeO_2 nanoparticles with palladium incorporated into the ceria lattice as $Pd_xCe_{1-x}O_{2-\delta}$ solid solution (E_b(Pd3$d_{5/2}$) = 338.0 eV). It was established that the greater relative proportion of palladium in oxide phase PdO was formed in the catalysts with higher palladium loading. The ratio between PdO and $Pd_xCe_{1-x}O_{2-\delta}$ phases is also controlled by the calcination temperature due to their strong interaction and dissolution of PdO nanoparticles inside ceria lattice. Also, TPR-CO showed the formation of low-temperature high reactive oxygen state, which was attributed to the surface compounds of palladium and ceria PdO_x(s)/Pd–O–Ce(s) characterized by E_b(Pd3$d_{5/2}$) = 336.1 eV.

It was proposed that catalytic activity in the low-temperature region (<100 °C) depends on a combination of two palladium species, the surface structures of PdO_x(s)/Pd–O–Ce(s) type and the $Pd_xCe_{1-x}O_{2-\delta}$ solid solution.

Acknowledgments

The work is supported by the Ministry of Education and Science of the Russian Federation (target grant for state support of leading universities of the Russian Federation #074-U01) and by Interdisciplinary Integration Project of SB RAS # 124.

Appendix A. Supplementary data

Supplementary material related to this article can be found, in the online version, at http://dx.doi.org/10.1016/j.apcatb.2014.11.015.

References

[1] A. Badri, C. Binet, J.-C. Lavalley, J. Phys. Chem. 100 (1996) 8363–8368.
[2] A. Bensalem, J.-C. Muller, D. Tessier, F. Bozon-Verduraz, J. Chem. Soc., Faraday Trans. 92 (1996) 3233–3237.
[3] P. Bera, K.C. Patil, V. Jayaram, G.N. Subbanna, M.S. Hegde, J. Catal. 196 (2000) 293–301.
[4] S.D. Senanayake, J. Zhou, A.P. Baddorf, D.R. Mullins, Surf. Sci. 601 (2007) 3215–3223.
[5] M. Cargnello, T. Montini, S. Polizzi, N.L. Wieder, R.J. Gorte, M. Graziani, P. Fornasiero, Dalton Trans. 38 (2010) 2122–2127.
[6] M.-F. Luo, X.-M. Zheng, Appl. Catal. A: Gen. 189 (1999) 15–21.
[7] J. Noh, O.B. Yang, D.H. Kim, S.I. Woo, Catal. Today 53 (1999) 575–582.
[8] W.-J. Shen, Y. Matsumura, J. Mol. Catal. A: Chem. 153 (2000) 165–168.
[9] K.R. Priolkar, P. Bera, P.R. Sarode, M.S. Hegde, S. Emura, R. Kumashiro, N.P. Lalla, Chem. Mater. 14 (2002) 2120–2128.
[10] M.S. Hegde, G. Madras, K.C. Patil, Acc. Chem. Res. 42 (2009) 704–712.
[11] E. Slavinskaya, R. Gulyaev, O. Stonkus, A. Zadesenets, P. Plyusnin, Y. Shubin, S. Korenev, A. Ivanova, V. Zaikovskii, I. Danilova, A. Boronin, Kinet. Catal. 52 (2011) 282–295.
[12] M.-F. Luo, Z.-Y. Hou, X.-X. Yuan, X.-M. Zheng, Catal. Lett. 50 (1998) 205–209.
[13] S.-H. Oh, G.B. Hoflund, J. Phys. Chem. A 110 (2006) 7609–7613.
[14] W.-J. Shen, Y. Matsumura, Phys. Chem. Chem. Phys. 2 (2000) 1519–1522.
[15] S. Roy, M.S. Hegde, Catal. Commun. 9 (2008) 811–815.
[16] S. Sharma, M.S. Hegde, R.N. Das, M. Pandey, Appl. Catal. A: Gen. 337 (2008) 130–137.
[17] P.A. Deshpande, M.S. Hegde, G. Madras, Appl. Catal. B: Environ. 96 (2010) 83–93.
[18] H. Zhu, Z. Qin, W. Shan, W. Shen, J. Wang, J. Catal. 233 (2005) 41–50.
[19] H. Zhu, Z. Qin, W. Shan, W. Shen, J. Wang, Catal. Today 126 (2007) 382–386.
[20] L. Meng, J.-J. Lin, Z.-Y. Pu, L.-F. Luo, A.-P. Jia, W.-X. Huang, M.-F. Luo, J.-Q. Lu, Appl. Catal. B: Environ. 119–120 (2012) 117–122.
[21] Y. Zhu, S. Zhang, J.-j. Shan, L. Nguyen, S. Zhan, X. Gu, F. Tao, ACS Catal. 3 (2013) 2627–2639.
[22] Y. Liu, T. Hayakawa, T. Ishii, M. Kumagai, H. Yasuda, K. Suzuki, S. Hamakawa, K. Murata, Appl. Catal. A: Gen. 210 (2001) 301–314.
[23] T. Baidya, G. Dutta, M.S. Hegde, U.V. Waghmare, Dalton Trans. 3 (2009) 455–464.
[24] I.G. Danilova, E.M. Slavinskaya, V.I. Zaikovskii, A.S. Ivanova, A.I. Boronin, R.V. Gulyaev, Y.I. Amosov, Kinet. Catal. 51 (2010) 143–148.
[25] A.I. Boronin, E.M. Slavinskaya, I.G. Danilova, R.V. Gulyaev, Y.I. Amosov, P.A. Kuznetsov, I.A. Polukhina, S.V. Koscheev, V.I. Zaikovskii, A.S. Noskov, Catal. Today 144 (2009) 201–211.
[26] E.M. Slavinskaya, A.I. Boronin, I.G. Danilova, Y.I. Amosov, A.S. Ivanova, P.A. Kuznetsov, I.A. Polukhina, R.V. Gulyaev, A.I. Stadnichenko, S.V. Koshcheev, V.I. Zaikovskii, A.S. Noskov, Kinet. Catal. 50 (2009) 819–823.
[27] W.J. Price, Analytical Atomic-Absorption Spectroscopy, Heyden & Son Ltd., London/New York/Rheine, 1972.
[28] S. Lowell, J.E. Shields, M.A. Thomas, M. Thommes, Characterization of Porous Solids and Powders: Surface Area, Pore Size and Density, Springer, Netherlands, 2006.
[29] L.S. Kibis, A.I. Stadnichenko, E.M. Pajetnov, S.V. Koscheev, V.I. Zaykovskii, A.I. Boronin, Appl. Surf. Sci. 257 (2010) 404–413.
[30] R.I. Kvon, A.I. Boronin, S.K. Shaikhutdinov, R.A. Buyanov, Appl. Surf. Sci. 120 (1997) 239–242.
[31] N.I. Baklanova, A.T. Titov, A.I. Boronin, S.V. Kosheev, J. Eur. Ceram. Soc. 26 (2006) 1725–1736.
[32] S. Krumm, Mater. Sci. Forum 183 (1996) 228.
[33] R.V. Gulyaev, A.I. Stadnichenko, E.M. Slavinskaya, A.S. Ivanova, S.V. Koscheev, A.I. Boronin, Appl. Catal. A: Gen. 439–440 (2012) 41–50.
[34] A. Gupta, M.S. Hegde, K.R. Priolkar, U.V. Waghmare, P.R. Sarode, S. Emura, Chem. Mater. 21 (2009) 5836–5847.
[35] S. Bernal, J.J. Calvino, M.A. Cauqui, J.M. Gatica, C. Larese, J.A. Pérez Omil, J.M. Pintado, Catal. Today 50 (1999) 175–206.
[36] V. Matolín, I. Matolínová, L. Sedláček, K.C. Prince, T. Skála, Nanotechnology 20 (2009) 215706.

[37] R.V. Gulyaev, T.Y. Kardash, S.E. Malykhin, O.A. Stonkus, A.S. Ivanova, A.I. Boronin, Phys. Chem. Chem. Phys. 16 (2014) 13523–13539.
[38] R.V. Gulyaev, E.M. Slavinskaya, S.A. Novopashin, D.V. Smovzh, A.V. Zaikovskii, D.Y. Osadchii, O.A. Bulavchenko, S.V. Korenev, A.I. Boronin, Appl. Catal. B: Environ. 147 (2014) 132–143.
[39] E.M. Slavinskaya, O.A. Stonkus, R.V. Gulyaev, A.S. Ivanova, V.I. Zaikovskii, P.A. Kuznetsov, A.I. Boronin, Appl. Catal. A: Gen. 401 (2011) 83–97.
[40] G.B. Hoflund, H.A.E. Hagelin, J.F. Weaver, G.N. Salaita, Appl. Surf. Sci. 205 (2003) 102–112.
[41] T. Pillo, R. Zimmermann, P. Steiner, S. Hüfner, J. Phys.: Condens. Matter 9 (1997) 3987–3999.
[42] S. Colussi, A. Gayen, M.F. Camellone, M. Boaro, J. Llorca, S. Fabris, A. Trovarelli, Angew. Chem. Int. Ed. 48 (2009) 8481–8484.
[43] M. Kurnatowska, L. Kepinski, W. Mista, Appl. Catal. B: Environ. 117–118 (2012) 135–147.
[44] L.S. Kibis, A.I. Stadnichenko, S.V. Koscheev, V.I. Zaikovskii, A.I. Boronin, J. Phys. Chem. C 116 (2012) 19342–19348.
[45] J. Allpress, J. Sanders, Aust. J. Phys. 23 (1970) 23–36.
[46] F. Giordano, A. Trovarelli, C. de Leitenburg, M. Giona, J. Catal. 193 (2000) 273–282.
[47] H. Zhu, Z. Qin, W. Shan, W. Shen, J. Wang, J. Catal. 225 (2004) 267–277.
[48] A.I. Titkov, A.N. Salanov, S.V. Koscheev, A.I. Boronin, Surf. Sci. 600 (2006) 4119–4125.
[49] A.S. Ivanova, E.M. Slavinskaya, R.V. Gulyaev, V.I. Zaikovskii, O.A. Stonkus, I.G. Danilova, L.M. Plyasova, I.A. Polukhina, A.I. Boronin, Appl. Catal. B: Environ. 97 (2010) 57–71.
[50] I. Danilova, E. Slavinskaya, V. Zaikovskii, A. Ivanova, A. Boronin, R. Gulyaev, Y. Amosov, Kinet. Catal. 51 (2010) 143–148.